INDIAN JOURNAL OF SCIENCE AND TECHNOLOGY

RESEARCH ARTICLE

Stagnation-Point Slip Flow of Hybrid Ferrofluid Past Exponentially Stretching Sheet in Darcy-Forchheimer Space

Sushil Prasad[1*], **Shilpa Sood**[2], **Archie Thakur**[3]

1 Research Scholar, Mathematics & Statistics, Career Point University, Hamirpur, Himachal Pradesh, India
2 Associate Professor, Mathematics & Statistics, Career Point University, Hamirpur, Himachal Pradesh, India
3 Assistant Professor, Department of Mathematics, CMR Institute of Technology, Bangalore, Karnataka, India

OPEN ACCESS

Received: 22-11-2023
Accepted: 22-01-2024
Published: 27-02-2024

Citation: Prasad S, Sood S, Thakur A (2024) Stagnation-Point Slip Flow of Hybrid Ferrofluid Past Exponentially Stretching Sheet in Darcy-Forchheimer Space. Indian Journal of Science and Technology 17(10): 881-890. https://doi.org/10.17485/IJST/v17i10.1910

* **Corresponding author**.

sushilprasad47@gmail.com

Funding: None

Competing Interests: None

Published By Indian Society for Education and Environment (iSee)

ISSN
Print: 0974-6846
Electronic: 0974-5645

Abstract

Objectives: The present article provides a detailed analysis on the Darcy-Forchheimer hybrid nanofluids flow past an exponentially stretching sheet in the presence of mixed convection with slip conditions and the impacts of different relevant parameters of the fluid flow for velocity and temperature profiles. **Methods:** In order to create hybrid nanofluids, two magnetic nanoparticles, magnetite (Fe_3O_4) and cobalt ferrite ($CoFe_2O_4$), are taken into consideration. The governing boundary layer coupled partial differential equations are transformed into a system of non-linear ordinary differential equations, which are then solved numerically by using the bvp4c solver available in the Matlab software. A comprehensive parametric analysis has been performed to show the effects of the convective parameter, velocity ratio parameter, porosity parameter, forchheimer parameter, solid volume fractions of Fe_3O_4 and $CoFe_2O_4$, velocity slip and temperature jump on the fluid velocity and temperature profiles as well as the local skin-friction coefficient and local Nusselt number within the boundary layer. **Findings:** For higher values of λ, ε, ϕ_1, ϕ_2, the velocity field grows, and it declines for γ, Fr, and A. The temperature field thickness is higher for γ, Fr, ϕ_1, ϕ_2 and A, while decreases for λ and ε. The local skin friction coefficient diminishes as rise in the values of ε, λ, γ, Fr, ϕ_1, ϕ_2, A and B. The local Nusselt number shows increasing behaviour for increasing amount of ε, λ, γ, Fr, ϕ_1, ϕ_2, A and B. **Novelty:** The novelty of the current work is the analysis of the flow of Darcy-Forchheimer hybrid nanofluids across an exponentially stretched sheet in the presence of mixed convection with slip conditions. Here, water is used as base fluid and magnetite, cobalt ferrite being used as hybrid nanoparticles for the present study.

Keywords: Hybrid nanofluids; Exponentially stretching sheet; Mixed convection; Velocity slip; Temperature jump

1 Introduction

An innovative approach to heat transmission is necessary to keep up with the latest technological developments. Hybrid nanofluids, which are an advanced category of fluids characterized by enhanced thermal properties, were recently discovered through nanofluid research. Dispersing nanocomposites or nanoparticles of various metals into the base fluid creates these fluids. When contrasted with nanofluids based on monoparticles and more traditional fluids, the hybrids exhibited superior thermal characteristics. A hybrid nanofluid's effectiveness and thermophysical properties may be affected by a number of factors, such as the ratio of nanoparticles, the stability of the hybrid nanofluid, the size of the nanoparticles, and the composition of the base fluid. Hybrid nanofluids have many real-world uses in engineering and industry, including the cooling of nuclear systems, electronics, biomedical applications, buildings (both heating and cooling), generators, engines, and thermal management systems for vehicles. They additionally serve to improve heat transfer technology, which in turn reduces costs in these fields [1,2].

Liaquat AliLund et al. [3] investigated the MHD outflow of the hybrid nanofluid. Hayat et al. [4] did research against the intensification of thermal conduction using hybrid nanofluid. Mabood et al. [5] explored hybrid nanofluid outflow together with melting transfer of heat. Aamir Ali et al.'s [6] study focused on boosting the thermal properties of a hybrid nanofluid composed of nanoparticles. Zhixiong Li and colleagues [7] statistically investigated the hydrothermal behavior as well as the irreversibility of hybrid nanofluid flows by means of a sinusoidal hairpin heat exchanger. Magnetite, cobalt, or iron micro-sized particles immersed in a liquid are known as ferrofluids. Typically, water or oil is utilized as the base fluid for ferrofluid. Ferrofluids exhibit superparamagnetism-like properties. It's because an external magnetic field has powerfully magnetized these fluids. A magnetic field can hold liquid seals formed by ferrofluids in place. NASA devised these liquids as a method of controlling the flow of rocket fuel in its orbit. Ferrofluids are beneficial for keeping dust off the magnetic disc drive's drive shafts as well. Ferrofluids can also be used to speed up the thermal transmission rate in a wide range of materials, as liquids are utilized in modern industry and technology. In the field of electronic and chemical devices, it is crucial.

When forced convection and natural convection mechanisms work together to transport heat, the technique is known as mixed convection or forced convection. This is usually referred to as circumstances in which buoyant and pressure forces interplay. Because of its significance in enhancing the thermal characteristics of heat transmission, mixed convection is one of the main areas of study for researchers. Additionally, it takes into consideration an instance of convection in general that emerges from a number of applications of technological advances and manufacturing in nature, along with the cooling of electronic devices, drying technology, the storage of solar energy, the manufacturing of foat glass, and the processing of food. A lot of research has been done on the mixed thermal transportation of nanofluids, as found in [8]. The stagnation-point fluid flow due to mixed convection finds its place in many applications like atmospheric boundary layer flows, nuclear collectors, solar collectors, heat exchangers, and so forth [1].

The permeability of porous media offers numerous benefits across a wide range of applications, such as fermentation, grain storage, groundwater pollution, reservoir dynamics, petroleum extraction, groundwater supply, fossil fuel operations, nuclear waste management, energy storage devices, oil reserves, solar panels, and many others. Darcy's [9] theory served as a foundation for numerous investigations concerning porous mediums characterized by low porosity and fluid velocities. However, it has certain drawbacks when applied to media with high permeability and greater transportability. At large flow speeds, conventional Darcy's law is inadequate in considering inertial and boundary conditions. Hence, Darcy's theory was inadequate in providing a rationale for physical conditions involving media with large porosities and velocities. To address this limitation, Forchheimer [10] proposed incorporating a square velocity component into the Darcy velocity model. This modification enables the analysis of inertia and boundary properties [11–15].

The focus of this research is to analyze the heat transfer rate of stagnated point hybrid nanofluid flow in the presence of mixed convection past an exponentially stretching sheet under slip conditions. The reason for choosing magnetite and cobalt ferrite nanoparticles in base fluid water is their capability of being used as a heat transfer fluid in many engineering and industrial applications like gas storage, atomic reactors, ultra-capacitors, heat transfer in solar and cooling devices, motors, and so forth. The one-phase model (Tiwari-Das model) is used in this study. Using similarity variables, the governing partial differential equations are transformed into ordinary differential equations, which are then numerically solved using Matlab software and computed using the bvp4c method. Numerous physical parameters have been calculated, and the impacts of velocity, temperature, skin friction, and Nusselt number have been presented graphically and through tables. Furthermore, the numerical data about physical quantities is tabulated and interpreted.

2 Methodology

Consider a continuous, incompressible and viscous hybrid ferrofluid, namely $Fe_3O_4 - CoFe_2O_4/H_2O$ of two-dimensional boundary layer with mixed convection at the stagnation point and slip effects across an exponentially stretching sheet. The

$x-$axis is chosen along the stretching surface in the flow direction, whereas the $y-$axis is orthogonal to surface. The sheet that stretches exponentially with velocity, $U_w(x) = ae^{x/L}$, where 'a' is a positive constant and 'L' be its characteristic length. The flow is sustained at constant temperature T_∞ and the velocity of free stream is,$U_\infty(x) = ce^{x/L}$ at some distance from the horizontal surface, where 'c' is positive constant. The temperature of surface is denoted by $T_w(x) = T_\infty + T_o e^{x/L}$, where '$T_\infty$' is average rate through which temperature expands across the sheet and 'T_∞' is the ambient temperature.

Because the hybrid nanofluids are created as stable combinations of the nanoparticles and the base fluids, the size of the nanoparticles is homogeneous, and the agglomeration impact of hybrid nanoparticles on the thermo physical characteristics is discarded. In order to synthesize the hybrid ferrofluids, magnetite Fe_3O_4 and cobalt ferrite $CoFe_2O_4$ ferroparticles are suspended in a water-based solution.

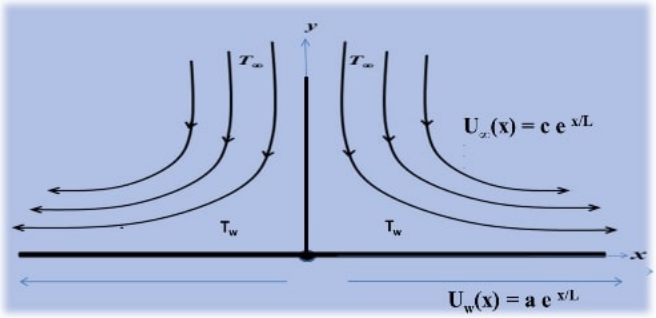

Fig 1. Schematic diagram of the flow

2.1 Governing Equations:

The basic boundary layer equations for the assumed model in cartesian coordinates x and y are given as: [see ref.s[1,2]]

$$\frac{\partial u}{\partial x} + \frac{\partial v}{\partial y} = 0, \tag{1}$$

$$u\frac{\partial u}{\partial x} + v\frac{\partial u}{\partial y} = U_\infty \frac{dU_\infty}{dx} + \frac{\mu_{hnf}}{\rho_{hnf}}\frac{\partial^2 u}{\partial y^2} + g\beta_{hnf}(T - T_\infty) + \frac{\nu_{hnf}}{k^*}\left(U_\infty - u^2\right) + F(U_\infty^2 - u^2), \tag{2}$$

$$u\frac{\partial T}{\partial x} + v\frac{\partial T}{\partial y} = \alpha_{hnf}\frac{\partial^2 T}{\partial y^2}, \tag{3}$$

The corresponding boundary conditions for current problem can be drafted as: [see ref.s[2] &[16]],

$$\begin{matrix} u = U_w(x) + A_1\dfrac{\partial u}{\partial y} = ae^{\dfrac{x}{L}} + A_1\dfrac{\partial u}{\partial y},\ v = 0, T = T_w(x) + B_1\dfrac{\partial T}{\partial y} & at\ y = 0, \\ u = U_\infty = ce^{\dfrac{x}{L}}, T \to T_\infty & as\ y \to \infty, \end{matrix} \tag{4}$$

where, A_1 and B_1 are the slip factors for velocity and thermal energy, respectively, 'g' stands for gravitational acceleration, β_{hnf} is the hybrid nanofluid's thermal expansion coefficient. Here ϕ_1 and ϕ_2 represents the concentration of Fe_3O_4 and $CoFe_2O_4$ ferroparticles in the base fluid H_2O respectively.

2.2 Similarity transformations:

The similarity transformations have been imposed following[17], given as:

$$\psi = \sqrt{2av_f L} f(\eta) e^{\frac{x}{2L}}, \eta = y\sqrt{\frac{a}{2v_f L}} e^{\frac{x}{2L}},$$
$$\theta(\eta) = \frac{T - T_\infty}{T_w - T_\infty}, \tag{5}$$

where ψ, v_f, and η denotes the respective stream function, kinematic viscosity, the similarity variable, whilst f and θ are dimensionless function. Next, we describe $u = \frac{\partial \psi}{\partial y}$, $v = -\frac{\partial \psi}{\partial x}$. While considering Equations (5) and (1) is identically satisfied. With the assistance of Equations (5), (2) and (3) are transformed as,

$$\frac{\mu_{hnf}/\mu_f}{\rho_{hnf}/\rho_f} f''' + ff''' - 2f'^2 + 2\varepsilon^2 + 2\lambda \frac{(\rho\beta)_{hnf}/(\rho\beta)_f}{\rho_{hnf}/\rho_f}\theta + \gamma(\varepsilon - f') + Fr(\varepsilon^2 - f'^2) = 0, \tag{6}$$

$$\frac{1}{Pr}\frac{k_{hnf}/k_f}{(\rho C_p)_{hnf}/(\rho C_p)_f}\theta'' + f\theta' - 4f'\theta = 0, \tag{7}$$

The transformed boundary conditions (Equation (4) 4) are:

$$\begin{aligned} &f(\eta) = 0\,,\ f'(\eta) = 1 + Af''(\eta)\,,\ \ \theta(\eta) = 1 + B\theta'(\eta) && at\ \eta = 0, \\ &f'(\eta) = \varepsilon\,,\ \theta(\eta) = 0 && as\ \eta \to \infty. \end{aligned} \tag{8}$$

Where prime symbolize differentiation w.r.t.η, and the dimensionless parameters are described as:
$A = A_1\left(\frac{\mu_{hnf}}{\rho_{hnf}}\right)e^{\frac{x}{2L}}\sqrt{\frac{a}{2Lv_f}}$ shows velocity slip parameter, $B = B_1\sqrt{\frac{a}{2Lv_f}}e^{\frac{x}{2L}}$ signifies thermal slip parameter, $\lambda = \frac{Gr_x}{Re_x^2}$ represents the thermal convection parameter, $\varepsilon = \frac{c}{a}$ depicts the velocity ratio parameter, $\gamma = \frac{2v_{hnf}L}{e^{x/L}k^* a}$ refers to the local porosity parameter, $Pr = \frac{v_f(\rho C_p)_f}{k_f}$ denotes the prandtl number and $Gr_x = \frac{g\beta_f(T_w - T_\infty)x^3}{v^2}$ represents thermal buoyancy parameter.

Table 1. Thermal and physical properties of magnetic nanoparticles and base fluid (see[18])

Physical properties	Fe_3O_4	$CoFe_2O_4$	Water
$\rho(kg/m^3)$	5180	4907	997.1
$C_p(J/kg.K)$	670	700	4179
$k(W/m.K)$	9.7	3.7	0.613
$\beta(K^{-1})$	1.3 x 10^{-5}	1.3 x 10^{-5}	21
$\mu(mPa/s)$	-	-	0.891
Pr	-	-	6.2

The models are being utilized for assessing the physical properties of nanofluid and hybrid nanofluid are introduced in Table 2.

Table 2. Thermal and physical properties of nanofluid & hybrid nanofluid (see[5])

Properties	Nanofluid	Hybrid Nanofluid
Density	$\rho_{nf} = (1-\phi_1)\rho_f + \phi_1\rho_{n1}$	$\rho_{hnf} = (1-\phi_2)\left[(1-\phi_1)\rho_f + \phi_1\rho_{n1}\right] + \phi_2\rho_{n2}$
Heat Capacity	$(\rho C_p)_{nf} = (1-\phi_1)(\rho C_p)_f + \phi_1(\rho C_p)_{n1}$	$(\rho C_p)_{hnf} = (1-\phi_2)\left[(1-\phi_1)(\rho C_p)_f + \phi_1(\rho C_p)_{n1}\right] + \phi_2(\rho C_p)_{n2}$
Thermal Conductivity	$k_{nf} = \frac{k_{n1}+2k_f-2\phi_1(k_f-k_{n1})}{k_{n1}+2k_f+\phi_1(k_f-k_{n1})}k_f$	$k_{hnf} = \frac{k_{n2}+2k_{nf}-2\phi_2(k_{nf}-k_{n2})}{k_{n2}+2k_{nf}+\phi_2(k_{nf}-k_{n2})}k_{nf}$

Continued on next page

Table 2 continued		
Thermal expansion coefficient	$(\rho\beta)_{nf} = (1-\phi_1)(\rho\beta)_f + \phi_1(\rho\beta)_{n1}$	$(\rho\beta)_{hnf} = (1-\phi_2)\left[(1-\phi_1)(\rho\beta)_f + \phi_1(\rho\beta)_{n1}\right] + \phi_2(\rho C_p)_{n2}$
Dynamic viscosity	$\mu_{nf} = \frac{\mu_f}{(1-\phi_1)^{2.5}}$	$\mu_{hnf} = \frac{\mu_f}{(1-\phi_1)^{2.5}(1-\phi_2)^{2.5}}$

Here, ϕ_1 and ϕ_2 denotes the nanoparticle concentrations of Fe_3O_4 and $CoFe_2O_4$, respectively in the base fluid H_2O. Base fluid, nanofluid, and hybrid nanofluid, all were denoted by letters f, nf *and* hnf, respectively. Similar to this, subscripts n_1 and n_2 have been used for nanoparticles of Fe_3O_4 and $CoFe_2O_4$, respectively.

2.3 Parameters of empirical importance:

For implementation in engineering and practical applications, the skin friction coefficient and Nusselt number, respectively, be defined as:

$$C_{fx} = \frac{\tau_w}{\rho_f U_w^2(x)}, \qquad Nu_x = \frac{xq_w}{k_f(T_w - T_\infty)},$$

Here τ_w represents shear stress over the surface of wall and q_w represents the heat flow from the wall. The expressions for these are illustrated as:

$$\tau_w = \mu_{hnf}\left(\frac{\partial u}{\partial y}\right)_{y=0}, \text{ and } q_w = -k_{hnf}\left(\frac{\partial T}{\partial y}\right)_{y=0},$$

As the dominant boundary conditions and similarity transformations are applied, Skin friction coefficient and local Nusselt number be defined in non-dimensional forms as:

$C_{fx}(2Re)^{\frac{1}{2}} = \frac{\mu_{hnf}}{\mu_f}(f''(\eta))_{\eta=0}$,

$Nu_x(Re_x/2)^{-\frac{1}{2}} = -\frac{k_{hnf}}{k_f}(\theta'(\eta))_{\eta=0}$,

i.e.

$C_{fx}(2Re)^{\frac{1}{2}} = \frac{1}{(1-\phi_1)^{2.5}(1-\phi_2)^{2.5}}(f''(\eta))_{\eta=0}$,

$Nu_x(Re_x/2)^{-\frac{1}{2}} = -\frac{k_{hnf}}{k_f}(\theta'(\eta))_{\eta=0}$,

where $Re_x = \frac{u_w(x)L}{\nu_f}$ depicts the Reynold's number.

2.4 Implementation of the bvp4c solver:

The bvp4c solver is an algorithm provided by MATLAB for solving BVPs. The design and implementation of the bvp4c solver were pioneered by Kierzenka and Shampine[19], who currently exhibit a tremendous amount of research on the subject. A descriptive implementation of bvp4c for the study under consideration has been mentioned here in this research. Using similarity transformations, we converted the set of PDEs to a set of ODEs and then computed the system using MATLAB's bvp4c solver. If we change the system of ODEs to a system of first order equations, then every boundary value problem may be formulated for its solution in bvp4c. Shampine[20] has provided the demonstration of the process. Steps I and II have explored the transformation of the system of ODEs for current research to a system of first-order equations. The boundary condition conversion is dealt with in step III, and step IV wraps up the remaining portion of the programme.

Step I: Firstly, we introduce a new set of variables for our coupled non-linear ODEs:

$f(1) = f,\ f(2) = f',\ f(3) = f'',\ f(4) = \theta,\ f(5) = \theta'$.

Step II: Here, some new variables into a set of Equations (6) and (7) and construct a structure of 1st order equation as:

$f'(1) = f(2)$

$f'(2) = f(3)$

$f'(3) = \frac{\rho_{hnf}/\rho_f}{\mu_{hnf}/\mu_f}\left(-ff'' + 2f'^2 - 2\varepsilon^2 - 2\lambda\frac{(\rho\beta)_{hnf}/(\rho\beta)_f}{\rho_{hnf}/\rho_f}\theta - \gamma(\varepsilon - f') - Fr(\varepsilon^2 - f'^2)\right)$

$f'(4) = f(5)$

$f'(5) = Pr\frac{(\rho C_p)_{hnf}/(\rho C_p)_f}{k_{hnf}/k_f}(-f\theta' + 4f'\theta)$

Step III: The boundary conditions have been transformed in accordance with the new variables as:$fa(1) = 0,\ fa(2) = 1 + Afa(3),\ fa(4)\ 1 + Bfa(5),\ fb(2) = \varepsilon,\ fa(4) = 0.$

Here, fa characterizes position at $\eta = 0$ and fb characterizes position as $\eta \to \infty$.

Step IV: To solve the set of first order equations together with boundary conditions, we use bvp4c solver in MATLAB software. For the first iteration of solution, we offered an initial guess along with a mesh size of 0.01.

3 Result and Discussion

The prime objective of this segment is to investigate the velocity and temperature profiles for various values of the relevant parameters. Using the bvp4c-technique, differential Equations (6) and (7) using boundary conditions (Equation (8)) are evaluated. In all of these computations, the value of Prandtl number has been set as 6.2. In this segment, the graphical and numerical findings are employed in order to precisely explore the impacts of pertinent factors upon velocity and temperature profiles. The impacts of various factors that governs dimensionless parameters, such as the velocity ratio parameter (ε), mixed convection parameter (λ), porosity parameter (γ), Forchheimer's parameter (Fr), solid volume fraction of Fe_3O_4 (ϕ_1), solid volume fraction of $CoFe_2O_4$ (ϕ_2), velocity slip parameter (A), and temperature slip parameter (B), are examined in this segment. The thermal and physical characteristics of base fluid and magnetic nanoparticles are displayed in Table 1. Table 2 demonstrate the physical characteristics of nanofluid and hybrid nanofluid, respectively. We compared our findings with a previously published work by Waini et al.[17] to verify the code and ensure that our results were accurate. In the Table 3, the values for $(2Re_x)^{1/2}C_{fx}$ and $(Re_x/2)^{-1/2}\,Nu_x$ are evaluated on account of distinct values of λ and ϕ_2 for Al_2O_3-Cu/H_2O where Pr = 6.2, $\phi_1 = 0.1$, and $\varepsilon = 1$. The Table 4 demonstrates how well the findings of the current study agree with those that have been published.

Table 3. A comparable study of values of $(2Re_x)^{1/2}\,C_{fx}$ and $(Re_x/2)^{-1/2}\,Nu_x$ for varying values of λ and ϕ_2 for Al_2O_3-Cu/H_2O, where Pr = 6.2, $\phi_1 = 0.1$, and $\varepsilon = 1$.

		Waini et al.[17]		Present Results	
λ	ϕ_2	$(2Re_x)^{1/2}C_{fx}$	$(Re_x/2)^{-1/2}\,Nu_x$	$(2Re_x)^{1/2}C_{fx}$	$(Re_x/2)^{-1/2}\,Nu_x$
-1	0	-1.986284	5.514729	-1.986120	5.514797
	0.02	-2.133358	5.642844	-2.133147	5.642935
	0.04	-2.282522	5.772345	-2.282262	5.772463
0	0	-1.666032	5.577035	-1.665882	5.577094
	0.02	-1.806661	5.707901	-1.806470	5.707979
	0.04	-1.949228	5.840119	-1.948997	5.840219
1	0	-1.357859	5.633659	-1.357718	5.633712
	0.02	-1.492592	5.766829	-1.492415	5.766899
	0.04	-1.629117	5.901308	-1.628903	5.901396

Table 4 depicted the local skin friction coefficient and local nusselt number variations with respect to velocity ratio parameter (ε), mixed convection parameter (λ), porosity parameter (γ), forchheimer's parameter (Fr), solid volume fraction of Fe_3O_4 (ϕ_1) and $CoFe_2O_4$ (ϕ_2), velocity slip parameter (A) and temperature slip parameter (B).

Table 4. Numerical results of Skin friction coefficient $-\frac{1}{(1-\phi_1)^{2.5}(1-\phi_2)^{2.5}}f''(\eta)$ and Nusselt number $-\frac{k_{hnf}}{k_f}\theta'(\eta)$ for the current study when Pr = 6.2

ε	λ	γ	Fr	ϕ_1	ϕ_2	A	B	$-\frac{1}{(1-\phi_1)^{2.5}(1-\phi_2)^{2.5}}f''(\eta)$	$-\frac{k_{hnf}}{k_f}\theta'(\eta)$
0.01	0.5	1	1	0.01	0.01	0.1	0.1	-1.4700	3.1848
0.02								-1.4640	3.1870
0.03								-1.4577	3.1893
0.04								-1.4712	3.1917
	0.6							-1.4527	3.1893
	0.7							-1.4356	3.1937
	0.8							-1.4186	3.1918
		1.5						-1.5705	3.1534
		2.0						-1.6627	3.1238
		2.5						-1.7479	3.0958
			1.5					-1.5298	3.1682
			2.0					-1.5860	3.1525
			2.5					-1.6389	3.1375
				0.02				-1.5176	3.2285
				0.03				-1.5661	3.2724
				0.04				-1.6155	3.3165
					0.02			-1.5163	3.2168

Continued on next page

Table 4 continued

	0.03		-1.5635	3.2489
	0.04		-1.6116	3.2813
		0.2	-1.2340	3.0557
		0.3	-1.0669	2.9530
		0.4	-0.9415	2.8684
		0.2	-1.4902	2.4374
		0.3	-1.5029	1.9749
		0.4	-1.5115	1.6602

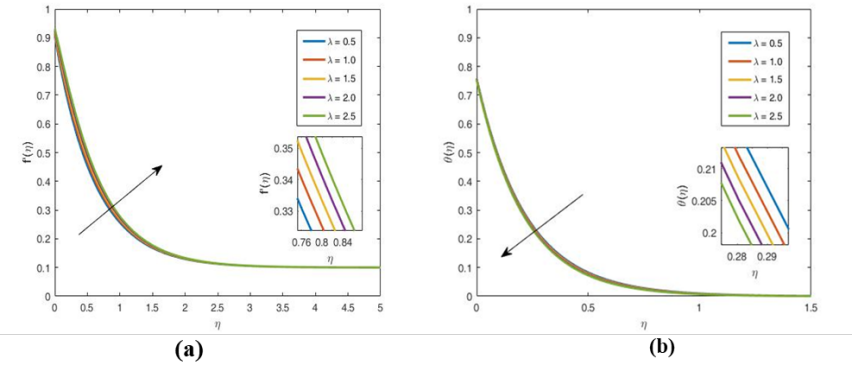

Fig 2. Effect of *Mixed Convection*(λ) **on** $f^{'}(\eta)$ **and** $\theta(\eta)$

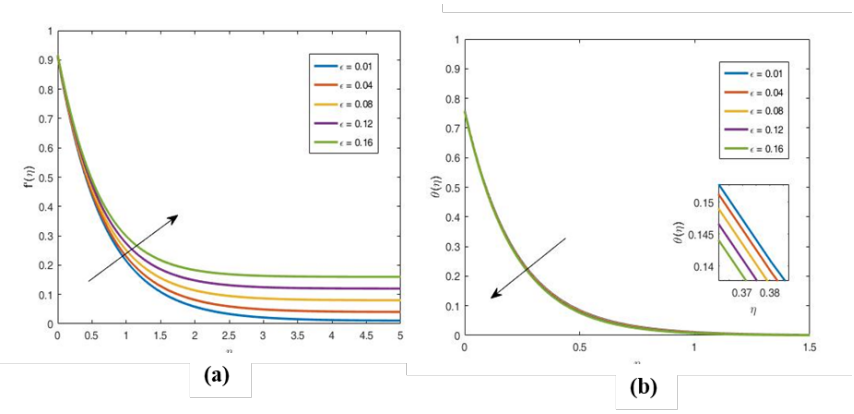

Fig 3. Effect of *velocity Ratio Parameter* (ε) **on** $f^{'}(\eta)$ **and** $\theta(\eta)$

Figure 2 illustrates how the convection parameter(λ) affect the velocity and temperature profile of the hybrid nanofluids. It is clear from the Figure 2**(a)**, that the velocity profiles tend to rise as λ increases. This is attributable to the way that a quicker pace of mixed convection brings about an expanded temperature contrast between the fluid and the region around the surface over which the fluid flows. This result is consent to the work done by[21]. The difference in the temperature permit to boost the velocity of the hybrid fluids. In Figure 2**(b)**, $\theta(\eta)$ diminishes although λ rises as it emphasize the difference in temperature between the fluid and the vicinity of surface. Therefore, the thickness of thermal boundaries gradually declines. Figure 3 portrays how the velocity ratio parameter (ε) affects velocity and temperature profile of the hybrid nanofluids. In general, velocity profile in Figure 3**(a)** tends to increase as ε value increases. As the value of the velocity ratio parameter expands, the fluid's velocity on the stretching sheet likewise increases, triggering the velocity boundary layer to enlarge and have good agreement with[1]. In Figure 3 **(b)**, $\theta(\eta)$ decreases as *velocity ratio parameter* (ε) increases. This is because due to the external velocity increases, heat is dispersed more quickly in the area, lowering fluid temperature.

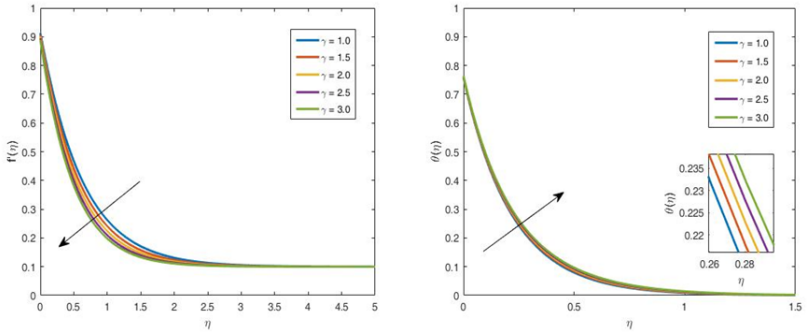

Fig 4. Effect of *Porosity Parameter* (γ) **on** $f^{'}(\eta)$ **and** $\theta(\eta)$

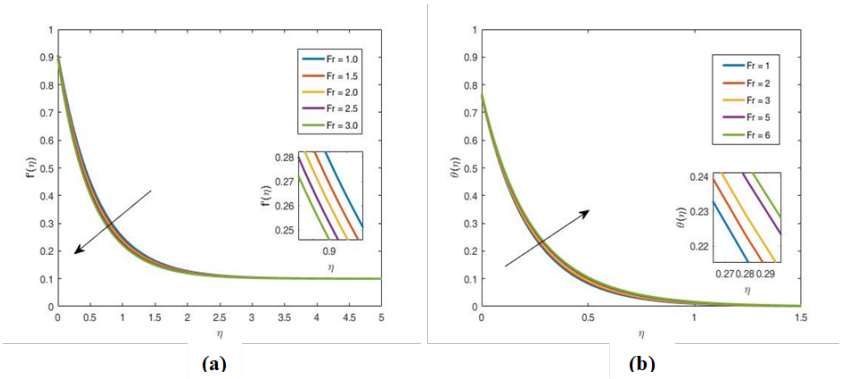

Fig 5. Effect of *Forchhemier number* (Fr) **on** $f^{'}(\eta)$ **and** $\theta(\eta)$

The schematic of Figure 4 shows how the velocity and temperature profile is affected by the porosity term (γ). Decay of $f^{'}(\eta)$ is caused by higher estimates of the local porosity parameter γ as seen in Figure 4**(a)**. The permeability of the fluid flow is substantially increased by the Darcy number and causes the fluid velocity to decrease since γ and the darcian drag force are inversely proportional to each other. Permeability enhancement causes the resistive force inside the particle to increase, which results in reducing the fluid's velocity. Also, Figure 4**(b)** displays the consequence of porosity parameter γ on temperature field $\theta(\eta)$. Higher estimates of γ are used to assess the intensification of the temperature field $\theta(\eta)$. Figure 5 depict the effects of the Forchhemier number (Fr) upon the velocity and temperature curves. In Figure 5**(a)**, improvements in the Forchhemier term curtail the velocity of fluid and boost the thermal energy profile in Figure 5 **(b)**. Such phenomena have been seen because the Forchhemier term lowers the permeability of the fluid. This result is in good agreement with [22].

The velocity profile for various slip parameter (A) values are listed in Figure 6**(a)**. In Figure 6**(a)**, it can be shown that the velocity profiles are a declining function of the slip parameter A. Physically, when a slip takes place, the surface skin friction between the sliding fluid and the stretching sheet decreases because not all of the stretching sheet's pulling force can be passed to the fluid. The fluid's velocity at the boundary layer will consequently decline when A is increased and is in good agreement with [23]. Also, Figure 6**(b)** depicts the impact of thermal slip parameter (B) on temperature profile. The temperature initially declines due to thermal slip parameter B, but beyond a certain distance from the sheet, this feature is smeared out. Due to a lesser amount of heat being transferred from the sheet to the fluid, it has been found that the temperature drops when the thermal slip parameter B is raised and have good consent with [24]. Figure 6 **(c)** shows how the temperature profile behaves for distinct values of Prandtl number (Pr). This graph clearly shows that a boost in Pr leads temperature profiles to decline and has an adverse impact on the thickness of the thermal boundary layer. This implies that heat will swiftly spread at higher Prandtl number extents. The fluid's thermal diffusivity grows as the Prandtl number does, which raises the fluid's temperature [11].

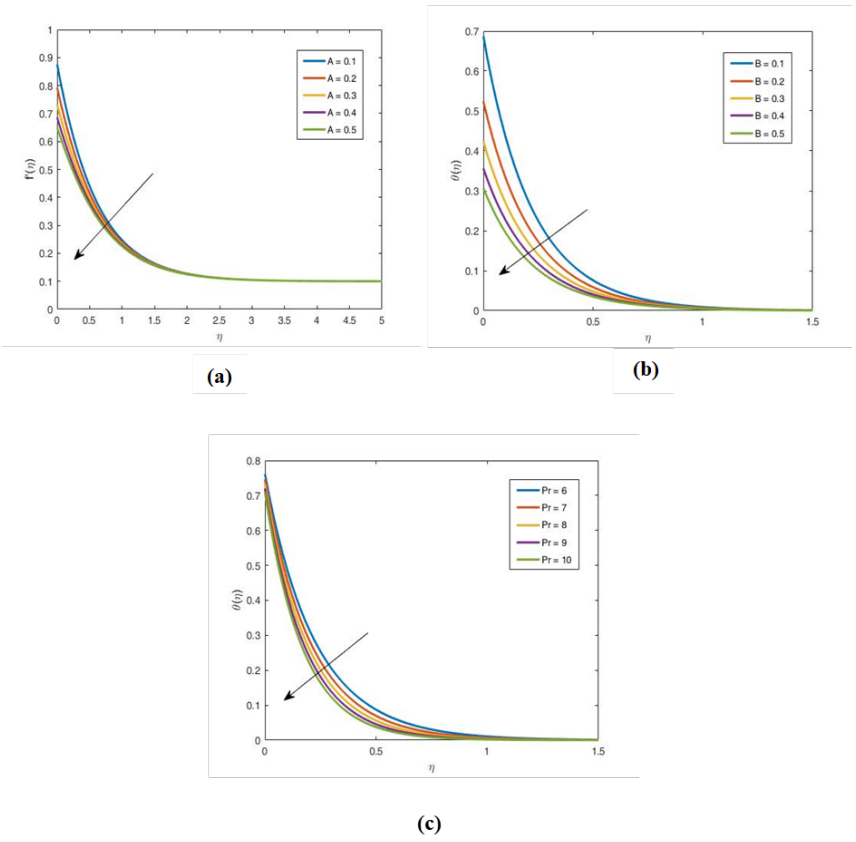

Fig 6. Effect of Slip parameter(A) on $f^{'}(\eta)$, Slip parameter(B) and Prandtl number(Pr) on $\theta(\eta)$

4 Conclusion

The Darcy-Forchheimer space and Stagnation-Point slip flow of Hybrid Ferrofluid Past Exponentially Stretching Sheet are examined in detail in this work and compared to previously published results. The impacts of mixed convection and slip parameters on two-dimensional boundary layer flows have been examined in this study. Future advancements in heat transfer rate can be achieved by a multifaceted strategy that includes the phenomena of mixed convection, velocity slip, and thermal leap. Understanding and controlling the dynamics of mixed convection—where forced and natural convection occur simultaneously—will be essential for optimizing thermal management in the transportation and electronics sectors. It is important to address the frequency of velocity slip at the boundaries between fluids and solids and efficiently control the transmission of heat across diverse material boundaries. Further research might focus on enhancing heat transfer efficiency by changing hybrid nanofluids with adaptive properties. Here are some notable aspects of this work:

- For higher values of λ, ε, ϕ_1, ϕ_2, the velocity field grows, and it declines for γ, Fr, and A.
- The temperature field thickness is higher for γ, Fr, ϕ_1, ϕ_2 and A, while decreases for λ and ε.
- Raising Prandtl number will lead to decrement in thermal boundary layer's thickness.
- As a consequence of the thermal slip, the temperature profile as well as accompanying thermal boundary layer's thickness drops.
- The local skin friction coefficient diminishes as rise in the values of ε, λ, γ, Fr, ϕ_1, ϕ_2, A and B.
- The local Nusselt number shows increasing behaviour for increasing amount of ε, λ, γ, Fr, ϕ_1, ϕ_2, A and B.

5 Nomenclature

BVP: Boundary value problem; ODE: Ordinary differential equation; PDE: Partial differential equation; β : Coefficient of thermal expansion; ε : Velocity ratio parameter; η : Dimensionless variable; λ : Thermal convection parameter; γ : Local

porosity parameter; Fr : Forcheimmer number; f : Dimensionless stream function; θ : Dimensionless temperature function; C_{fx} : Skin friction coefficient; Nu_x : Nusselt number; Re_x : Reynold's number; Pr : Prandtl's number; A: Velocity slip parameter; B: Temperature slip parameter; α : Thermal diffusivity; k : Thermal conductivity; μ : Dynamic viscosity; ν : Kinematic viscosity; ρ : Density; τ_w : Shear stress at the wall ; a, c : Positive constant for stretching rate; C_p : Specific heat at constant pressure; g: Acceleration due to gravity; k^* : Permeability; q_w : Heat flux; T : Absolute free temp. of the fluid; T_w : The temp. of the stretching surface; T_∞ : The temp. of the free stream; U_w : The stretching velocity at surface; U_∞ : Free stream velocity of the fluid; u, v: Horizontal and vertical velocity comp; x, y : Cartesian coordinates

References

1) Thakur A, Sood S. Comparative investigation of the mixed convective stagnated flow of hybrid nanofluids past an exponentially stretching sheet. *ZAMM-Journal of Applied Mathematics and Mechanics/Zeitschrift für Angewandte Mathematik und Mechanik*. 2022;102(12):1–14. Available from: https://doi.org/10.1002/zamm.202100419.
2) Anuar NS, Bachok N, Arifin NM, Rosali H, Pop I. Stagnation-Point Flow and Heat Transfer Over an Exponentially Stretching/Shrinking Sheet in Hybrid Nanofluid with Slip Velocity Effect: Stability Analysis. In: 2nd International Conference on Applied & Industrial Mathematics and Statistics ;vol. 1366 of Journal of Physics: Conference Series. IOP Publishing. 2019;p. 012002–012002. Available from: https://iopscience.iop.org/article/10.1088/1742-6596/1366/1/012002.
3) Lund LA, Omar Z, Raza J, Khan I. Magnetohydrodynamic flow of Cu–Fe3O4/H2O hybrid nanofluid with effect of viscous dissipation: dual similarity solutions. *Journal of Thermal Analysis and Calorimetry*. 2021;143:915–927. Available from: https://doi.org/10.1007/s10973-020-09602-1.
4) Hayat T, Nadeem S, Khan AU. Numerical analysis of Ag-CuO/water rotating Hybrid nanofluid with heat generation/absorption. *Canadian Journal of Physics* . 2018;97(2):644–650. Available from: https://doi.org/10.1139/cjp-2018-0011.
5) Mabood F, Yusuf TA, Khan WA. Cu-Al2O3 –H2O Hybrid Nanofluid flow with melting heat transfer, Irreversibility Analysis and Non-Linear Thermal Radiation. *Journal of Thermal Analysis and Calorimetry* . 2021;143:973–984. Available from: https://doi.org/10.1007/s10973-020-09720-w.
6) Ali A, Noreen A, Saleem S, Aljohani AF, Awais M. Heat transfer analysis of Cu–Al2O3 hybrid nanofluid with heat flux and viscous dissipation. *Journal of Thermal Analysis and Calorimetry* . 2020;143(3):2367–2377. Available from: https://doi.org/10.1007/s10973-020-09910-6.
7) Li Z, Shahsavar A, Niazi K, Al-Rashed AAAA, Rostami S. Numerical assessment on the hydrothermal behavior and irreversibility of MgO-Ag/water hybrid nanofluid flow through a sinusoidal hairpin heat-exchanger. *International Communications in Heat and Mass Transfer*. 2020;115:104628. Available from: https://doi.org/10.1016/j.icheatmasstransfer.2020.104628.
8) El-Zahar ER, Rashad AM, Saad W, Seddek LF. Magneto-Hybrid Nanofluids Flow via Mixed Convection past a Radiative Circular Cylinder. *Scientific Reports*. 2020;10(1):1–13. Available from: https://doi.org/10.1038/s41598-020-66918-6.
9) Darcy H. Les fontaines publiques de la ville de Dijon. Dalmont V, editor. 1856. Available from: https://books.google.co.in/books/about/Les_fontaines_publiques_de_la_ville_de_D.html?id=42EUAAAAQAAJ&redir_esc=y.
10) Forchheimer P. Wasserbewegung durch boden. In: Zeitschrift des Vereines Deutscher Ingenieure;vol. 45. 1901;p. 1781–1788. Available from: https://cir.nii.ac.jp/crid/1572261549273889536.
11) Sharma S. MHD Boundary Layer Flow Past an Exponentially Stretching Sheet with Darcy-Forchheimer Flow of Nanofluids. *Indian Journal Of Science And Technology*. 2022;15(33):1594–1604. Available from: https://doi.org/10.17485/IJST/v15i33.607.
12) Zainodin S, Jamaludin A, Nazar R, Pop I. MHD Mixed Convection of Hybrid Ferrofluid Flow over an Exponentially Stretching/Shrinking Surface with Heat Source/Sink and Velocity Slip. *Mathematics*. 2022;10(23):1–20. Available from: https://doi.org/10.3390/math10234400.
13) Asghar A, Chandio AF, Shah Z, Vrinceanu N, Deebani W, Shutaywi M, et al. Magnetized mixed convection hybrid nanofluid with effect of heat generation/absorption and velocity slip condition. *Heliyon*. 2023;9(2):1–13. Available from: https://doi.org/10.1016/j.heliyon.2023.e13189.
14) Ullah Z, Zari I, Gul T, Ali I, Alghamdi WI, Ali F. Darcy-Forchheimer hybrid nanofluids flow with quadratic convection over a stretched tube. *Advances in Mechanical Engineering*. 2023;15(6):1–10. Available from: https://doi.org/10.1177/16878132231180866.
15) Gohar, Khan TS, Sene N, Mouldi A, Brahmia A. Heat and Mass Transfer of the Darcy-Forchheimer Casson Hybrid Nanofluid Flow due to an Extending Curved Surface. *Journal of Nanomaterials*. 2022;2022:1–12. Available from: https://doi.org/10.1155/2022/3979168.
16) Zainodin S, Jamaludin A, Nazar R, Pop I. MHD Mixed Convection of Hybrid Ferrofluid Flow over an Exponentially Stretching/Shrinking Surface with Heat Source/Sink and Velocity Slip. *Mathematics*. 2022;10(23):1–20. Available from: https://doi.org/10.3390/math10234400.
17) Waini I, Ishak A, Pop I. Hybrid nanofluid flow induced by an exponentially shrinking sheet. *Chinese Journal of Physics*. 2020;68:468–482. Available from: https://doi.org/10.1016/j.cjph.2019.12.015.
18) Kopp MI, Yanovsky VV, Anusha T, Mahabaleshwar US. MHD Flow and Heat Transfer of a Ternary Hybrid Ferrofluid Over a Stretching/Shrinking Porous Sheet with the Effects of Brownian Diffusion and Thermophoresis. *East European Journal of Physics*. 2023;(1):7–18. Available from: https://doi.org/10.26565/2312-4334-2023-1-01.
19) Kierzenka J, Shampine LF. A BVP solver based on residual control and the Maltab PSE. *ACM Transactions on Mathematical Software*. 2001;27(3):299–316. Available from: https://doi.org/10.1145/502800.502801.
20) Shampine LF, Kierzenka J, Reichelt MW. Solving Boundary Value Problems for Ordinary Differential Equations in Matlab with bvp4c. 2000. Available from: https://citeseerx.ist.psu.edu/document?repid=rep1&type=pdf&doi=545dfa145ebf948b2cd7e5a90cf00df476dc69a1.
21) Jafar AB, Shafie S, Ullah I, Safdar R, Jamshed W, Pasha AA, et al. Mixed convection flow of an electrically conducting viscoelastic fluid past a vertical nonlinearly stretching sheet. *Scientific Reports*. 2022;12(1):1–13. Available from: https://doi.org/10.1038/s41598-022-18761-0.
22) Devi R, Sood S. Numerical Analysis of the Influence of an Inclined Magnetic Field on the Flow of Casson Nanofluid Across an Exponentially Stretching Surfae, using the Darcy-Forchheimer model. *Indian Journal Of Science And Technology*. 2023;16(44):4081–4089. Available from: https://doi.org/10.17485/IJST/v16i44.2481.
23) Sharma S, Dadheech A, Parmar A, Arora J, Al-Mdallal Q, Saranya S. MHD micro polar fluid flow over a stretching surface with melting and slip effect. *Scientific Reports*. 2023;13(1):1–15. Available from: https://doi.org/10.1038/s41598-023-36988-3.
24) Trivedi M, Otegbeye O, Ansari MS, Fayaz T. Impact of thermal jump condition on Jeffrey fluid flow consisting nanoparticles: An unsteady case. *International Journal of Thermofluids*. 2023;18:1–10. Available from: https://doi.org/10.1016/j.ijft.2023.100331.